Hernández, A., et al., 2020, External forcing mechanisms controlling the North Atlantic coastal upwelling regime during the mid-Holocene: Geology, v. 49, https://doi.org/10.1130/G48112.1

Supplemental Material

External forcing mechanisms controlling the North Atlantic coastal upwelling regime during the mid-Holocene

Armand Hernández, Mário Cachão, Pedro Sousa, Ricardo M. Trigo, Jürg Luterbacher, José M. Vaquero, Maria C. Freitas

- *Setting and Previous Work*

Located on the south-western coast of Portugal (37° 40'N, 8° 40' W) and 30 km south of Sines in the Alentejo coast, the Corgo do Porto is a small tributary on the right bank of the Mira River, outleting 3.5 km upstream of its mouth. The Mira estuary is a small mesotidal system with a semidiurnal tidal regime (Adão et al., 2009). It is formed by a single channel, 5–10 m deep and a maximum width of 400 m, which allows tidal influence to extend 40 km upstream (Bonaventura et al., 1999). Its basin is essentially developed on Paleozoic formations (greywakes, pelites, shales and conglomerates), although there are also Plio-Pleistocene sands, sandstones and conglomerates, Pliocene siltstones and Holocene dune and beach sands in the area (Loureiro et al., 2009). The Mira estuarine system has a total area of 5 km^2, a mean depth of 4 m and a volume of 27 x 10^{-6} m^3. Its mean river flow, residence time and tidal range are 3 m^3 s^{-1}, 15 days and 2.4 m, respectively (França et al., 2009). Due to the low, seasonal and limited freshwater input, the lower section of the estuary has a dominant marine signature and is characterized by extensive *Z. noltii* meadows, bare sandy areas and muddy substrates, with salt-marshes occurring as far as 20 km upstream (Amaral and Paula, 2007). The valley is flat-floored due to terrigenous siltation and forms an alluvial plain reclaimed for agriculture/aquaculture. Nevertheless, these conditions were quite distinct in the recent past because of extensive marine flooding of this area during the high-rate positive eustatism that followed the Last Glacial Maximum (Alday et al., 2006).

The sedimentary infill of the Corgo do Porto alluvial plain was characterized by the lithological description and the multiproxy analysis of the MIRA-CP1 core obtained in 2002 (Alday et al., 2006). From the bottom to the top of the core four sedimentary units (units I to IV) were identified (Fig. S1). Unit I consist of muddy sand and sandy mud, with shale and quartz angular pebbles, mildly to strongly alkaline, free of carbonate and with traces of organic matter. The boundaries separating layers are usually gradual and diffuse. The sandy fraction is generally coarse, poorly sorted and negatively skewed, suggesting the presence of small contributions of coarser lag. Unit II is homogeneous and consists of a monotonous sequence of grey sandy mud alternating with grey mud, free of pebbles. Throughout this unit bioclasts are abundant. Sediment is moderately alkaline and OM content ranges between 2 and 6%. The contact with Unit III is erosive. Unit III consists of alternating grey mildly alkaline slightly muddy sand and grey neutral muddy sand. The sand fraction of the former is coarse and of the latter is medium. The organic matter content ranges between 1 and 7%, with higher values associated to finer sediment. The carbonate fraction is usually <10% but it can reach punctually 16%. Unit IV shows a fining upward

trend, with a sequence of brown sandy mud, slightly sandy mud and mud, topped by an accumulation of plant debris mixed with silt and clay. The sand fraction is finer in comparison to the equivalent component in Units I and III. These sediments are strongly to extremely acid and free of carbonate. The organic matter content ranges from 3 to 7%, except for the topmost 3 cm, where it reaches 32%. From bottom upwards depositional environments were interpreted as: i) lower fluvial (no nannolith content); ii) lower estuarine (sparse nannolith content); iii) paleo-ria (with rich and continuous nannolith assemblages); iv) upper estuarine (returning to sparse nannolith content) and v) upper fluvial sequence (no nannolith content).

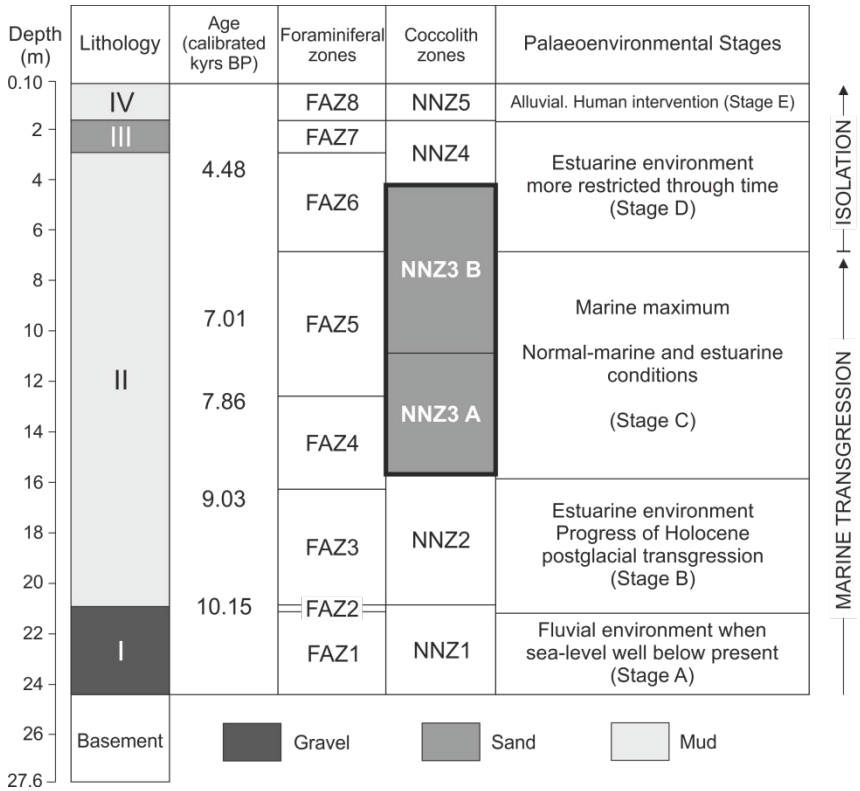

Figure S1: Summary of lithostratigraphic units, micropaleontological zones and paleoenvironmental stages throughout the MIRA-CP1 core (modified from Alday et al., 2006)

- *Chronological Framework*

Five samples consisting of organic mud or wood were dated using AMS (accelerated mass spectrometry) 14C radiometric technique by Beta Analytic Inc., USA (Table S1) and calendar calibration followed the database and procedure given by Stuiver et al. (1998). Alday et al. (2006) estimated ages for other samples by linear interpolation assuming constant sedimentation rates between dated points. Here, the age–depth model was upgraded applying Bacon 2.2 software (Blaauw and Christen, 2011) (Fig. S2), however results do not differ significantly (max. difference between samples < 10 years).

Table S1: Radiocarbon ages from MIRA-CP1 core (Adapted from Alday et al., 2006)

Radiocarbon dates

Laboratory code	Depth (m)	Material	$\delta^{13}C$ (%)	Conventional ^{14}C years BP	Calendar calibrated age BP	2σ calibrated BP
Beta-181358	-3.04	Organic sediment	-25.4	4020	4475	4595 - 4405
Beta-167493	-9.42	Organic sediment	-25.9	6160	7010	7220 - 6900
Beta-181920	-12.46	Organic sediment	-23.2	7050	7860	7960 - 7765
Beta-181359	-16.35	Organic sediment	-25.3	8140	9030	9250 - 9000
Beta-181360	-20.71	Organic sediment	-25.8	8920	10,150	10,200 - 9900

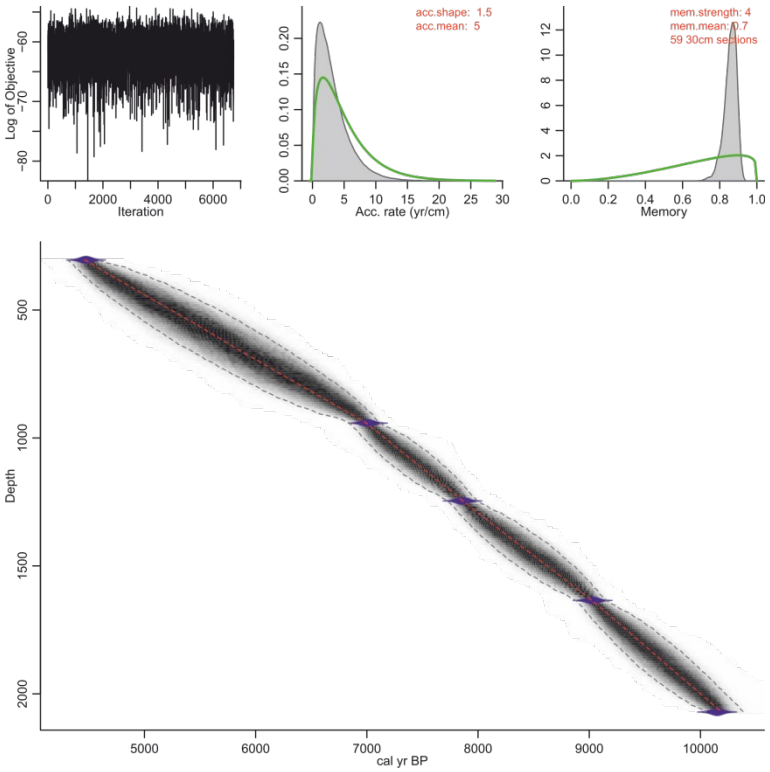

Figure S2: Age–depth model for sediment core MIRA-CP1 constructed using Bacon 2.2 software (Blaauw and Christen, 2011).

- *Nannoliths Analysis*

Sixteen calcareous nannofossil (calcareous nannoplankton and didemnid ascidian spicules) taxa were identified throughout MIRA-CP1 core (see Alday et al. (2006) for further details). Based on the species presence, abundance, diversity and dominance, the MIRA-CP1core (ca. 25 m thick) was previously divided into five different nannofossil zones (NNZ; Alday et al. (2006)). However, for the purpose of this work only samples from the marine calcareous nannofossil Zone 3 (NNZ 3) have been taken into account.

NNZ3 (16 m to 4.05 m) is characterized by high and persistent record on nannoliths (Fig. S3). This zone can be further divided in two subzones: NNZ3A (16 m to 11.06 m), characterized by the relative dominance of *Gephyrocapsa oceanica, Gephyrocapsa muellerae, Umbilicosphaera sibogae, Syracosphaera histrica-pulchra, Coronosphaera mediterranea* and a dominance cycle of *Coccolithus pelagicus braarudi* and *Calcidiscus leptoporus*; and NNZ3B (11.06 m to 4.05 m),

characterized by the relative dominance of *Helicosphaera carteri, Braarudosphaera bigelowii* together with ascidian spicules and a second dominance cycle of *C. pelagicus braarudi* and *Calcidiscus leptoporus*.

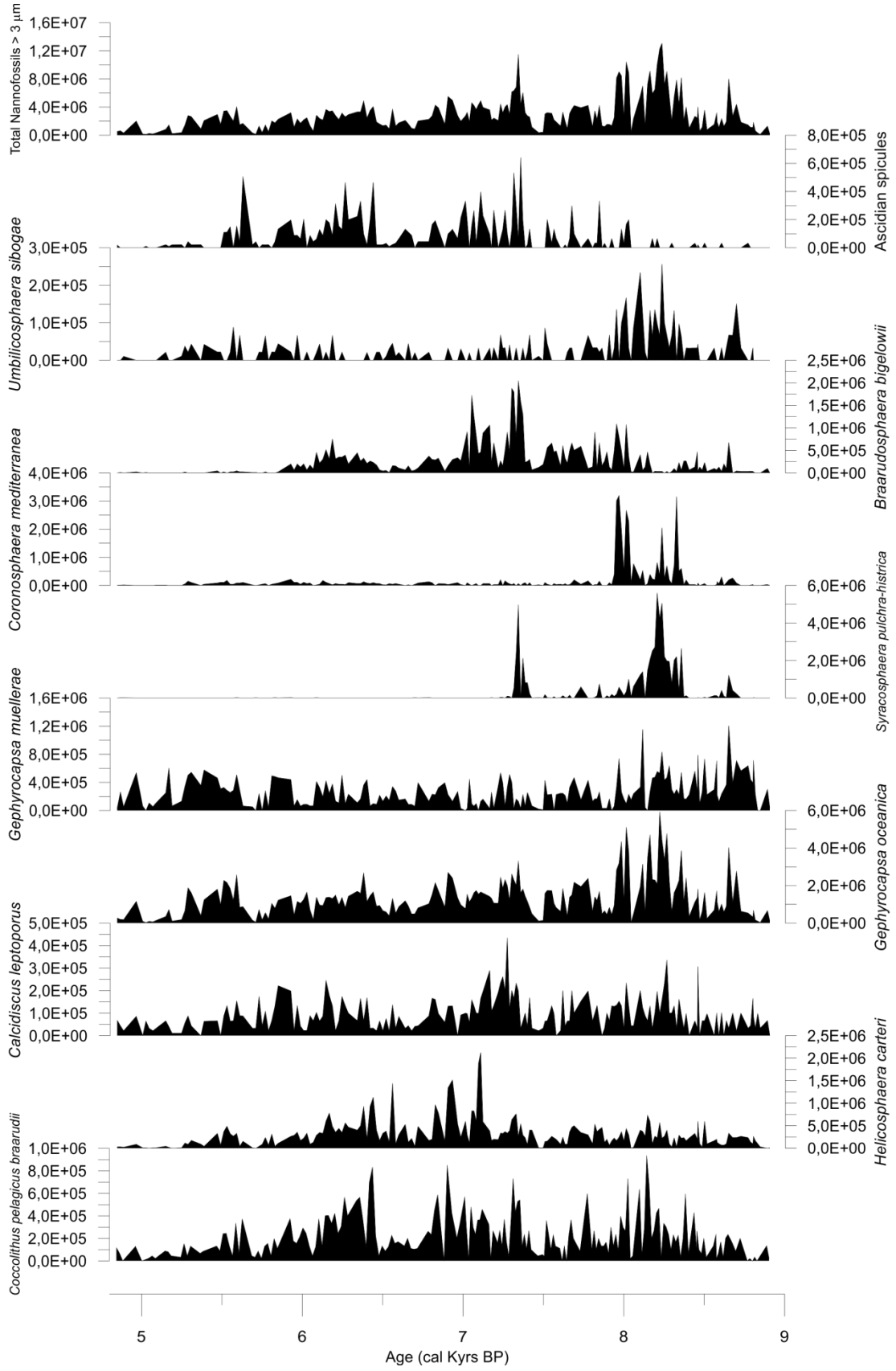

Figure S3: Absolute abundance of nannoliths per gram of sediment from the MIRA-CP1 core.

- *Orbital and Solar Activity Forcing*

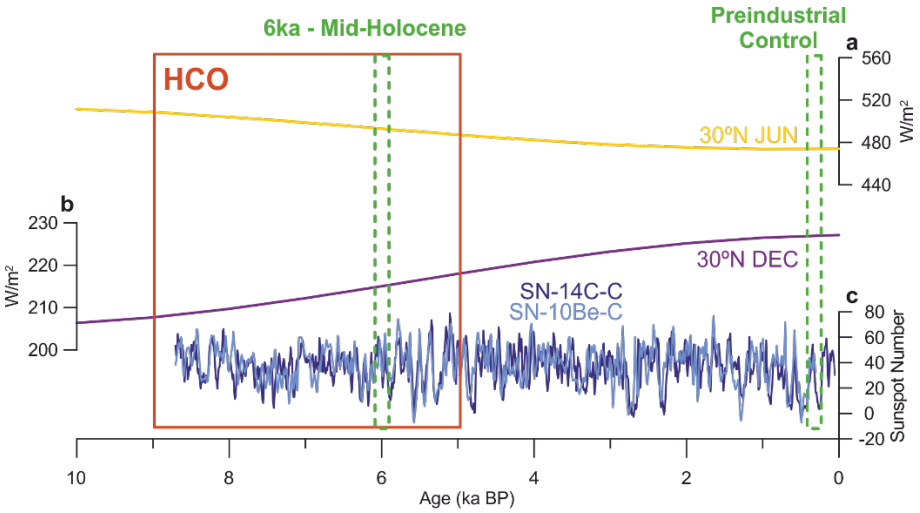

Figure S4: Solar insolation owing to orbital changes through the last 10k years BP for 30°N during the (a) summer and (b) winter by Berger and Loutre (1991) (c) Sunspot number reconstructions SN-14C-C and SN-10Be-C (dark- and light-blue lines, respectively) by Usoskin et al. (2016). Green rectangles represent the Preindustrial control period and the mid-Holocene from where the steady forcing conditions for model simulations were taken. Red rectangle indicates the time window corresponding to the proxy-based data of this study.

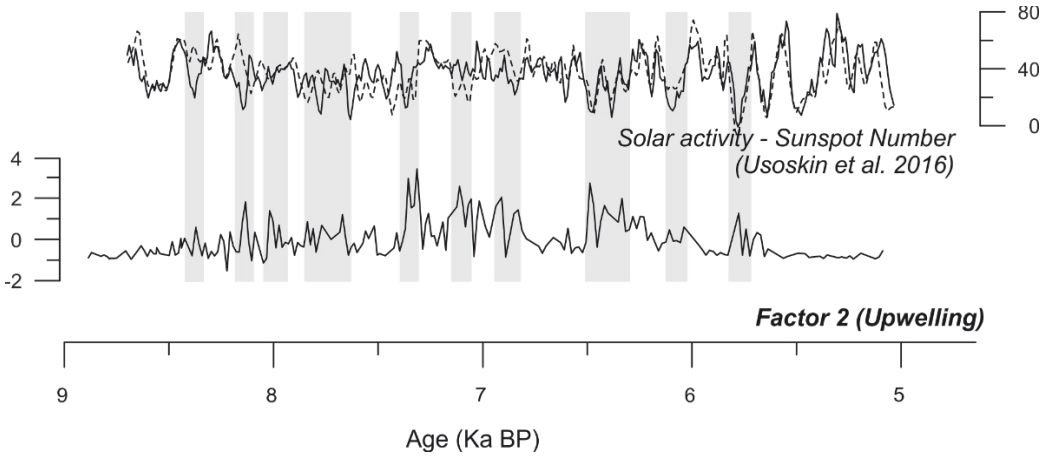

Figure S5: Comparison of upwelling index and sunspot number proxy-based reconstructions. Black thin and discontinuous black lines represent 14C and 10Be sunspot number reconstructions, respectively. Gray bands show low sunspot number values and enhanced upwelling conditions.

- *Model Simulations*

We computed the bulk Upward Mass Transport in a layer between the surface and approximately 150 meters deep in each gridpoint, and then compared the difference between the 6k yr BP and the preindustrial control period simulations. This was made for each individual model, and also for an ensemble mean of the 4 models which have this variable (Table S2 and Fig. S5).

For the surface radiative budget, we computed the sum of longwave and shortwave radiative fluxes at the surface for each period (6k yrs BP and preindustrial control period) and then the difference for the budgets between the two simulations. This was made for each individual model, and also for an ensemble mean of the 5 models which have this variable (Table S2 and Fig. S6).

For the mean sea level pressure, sea surface temperature, 2 meter above ground temperature and 10 m above ground wind we compared the difference between the 6k yr BP and the pre-industrial control period simulations. This was made for each individual model, and also for an ensemble mean of the 5 models which have this variable (Table S2 and Fig. S7, S8 and S9).

Table S2: List of models and their main characteristics. Variables: slp – mean sea level pressure; rlds – downward longwave radiation flux at surface; rsds – downward shortwave radiation flux at surface; uas – near-surface zonal wind component; vas – near-surface meridional wind component; tos – sea surface temperature; wmo – upward water mass transport.

Model Name	Horizontal Resolution (Atmosphere)	Horizontal Resolution (Ocean)	Ensemble Code	Variables	Reference
BCC_CSM1.1	64 x 128	232 x 360	r1i1p1	slp, rlds, rsds, uas, vas, tos, wmo	Xin et al. 2013
CCSM4	192 x 288	320 x 384	r1i1p1	slp, rlds, rsds, uas, vas, tos, wmo	Gent et al. 2011
IPSL-CM5A-LR	96 x 97	149 x 182	r1i1p1	slp, rlds, rsds, uas, vas, tos, wmo	Dufresne et al. 2013
MIROC-ESM	64 x 128	129 x 192	r1i1p1	slp, rlds, rsds, uas, vas, tos	Sueyoshi et al. 2013
MRI-CGCM3	160 x 320	360 x 368	r1i1p1	slp, rlds, rsds, uas, vas, tos, wmo	Yukimoto et al. 2012

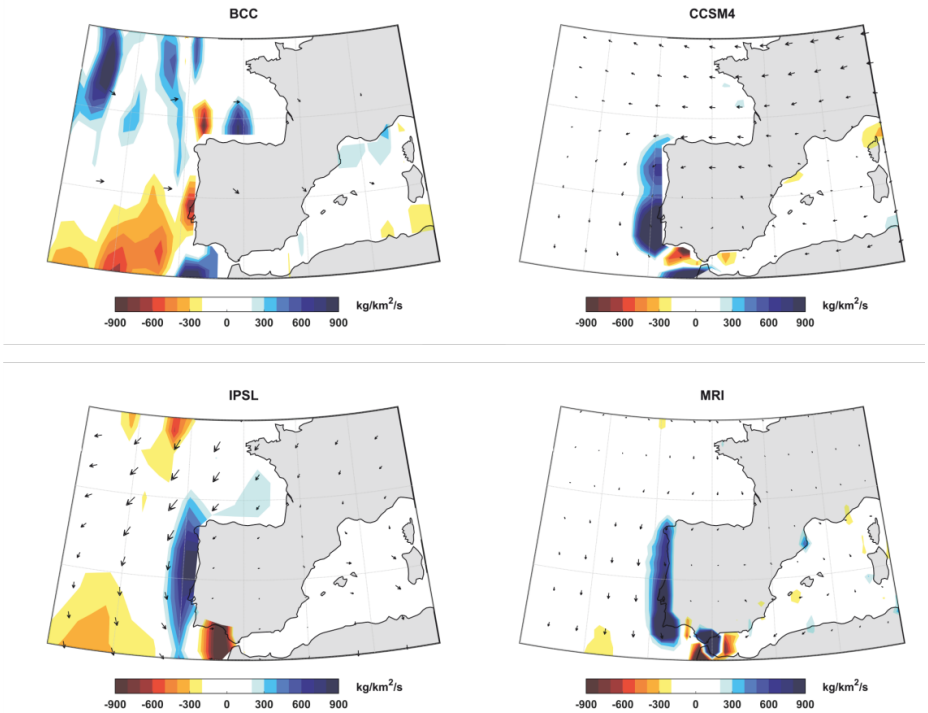

Figure S6: Anomalies in the summer Upward Mass Transport of water in the 0-150 m layer (shaded) and in surface wind (vectors) over the INAM during the mid-Holocene (when compared to the pre-industrial control period) from four atmosphere-ocean coupled general circulation models (CGCMs) that contributed to the third phase of the Paleoclimate Modelling Intercomparison Project (PMIP3; Braconnot et al. 2012) within the scope of CMIP5. These models are: (i) BCC-CSM1.1 (Xin et al. 2013), (ii) CCSM4 (Gent et al. 2011), (iii) IPSL-CM5A-LR (Dufresne et al. 2013) and (iv) MRI-CGCM3 (Yukimoto et al. 2012).

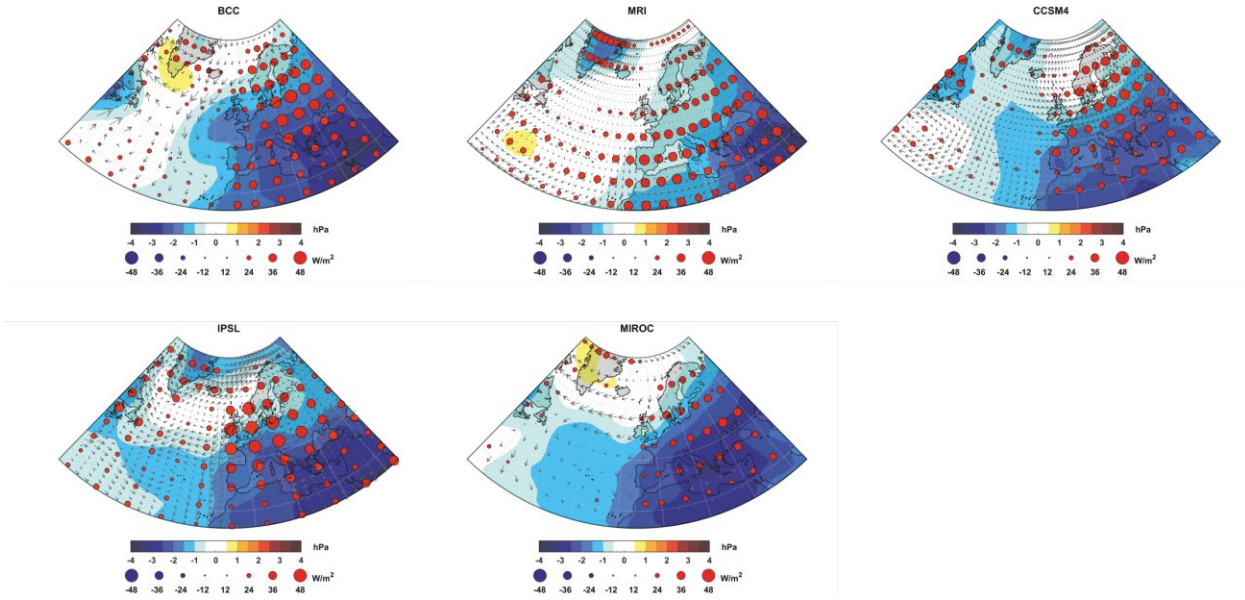

Figure S7: Anomalies in the summer surface radiative budget (circles), summer mean sea level pressure (shaded) and summer surface wind (vectors) over the North Atlantic region during the mid-Holocene (when compared to the pre-industrial control period) from five atmosphere-ocean coupled general circulation models (CGCMs) that contributed to the third phase of the Paleoclimate Modelling Intercomparison Project (PMIP3; Braconnot et al. 2012) within the scope of CMIP5. These models are: These models are (i) BBC-CSM1 (Xin et al. 2013), (ii) (v) MRI-CGCM3 (Yukimoto et al. 2012), (iii) CCSM4 (Gent et al. 2011), (iv) IPSL-CMA-MR (Dufresne et al. 2013) and (v) MIROC-ESM (Sueyoshi et al. 2013).

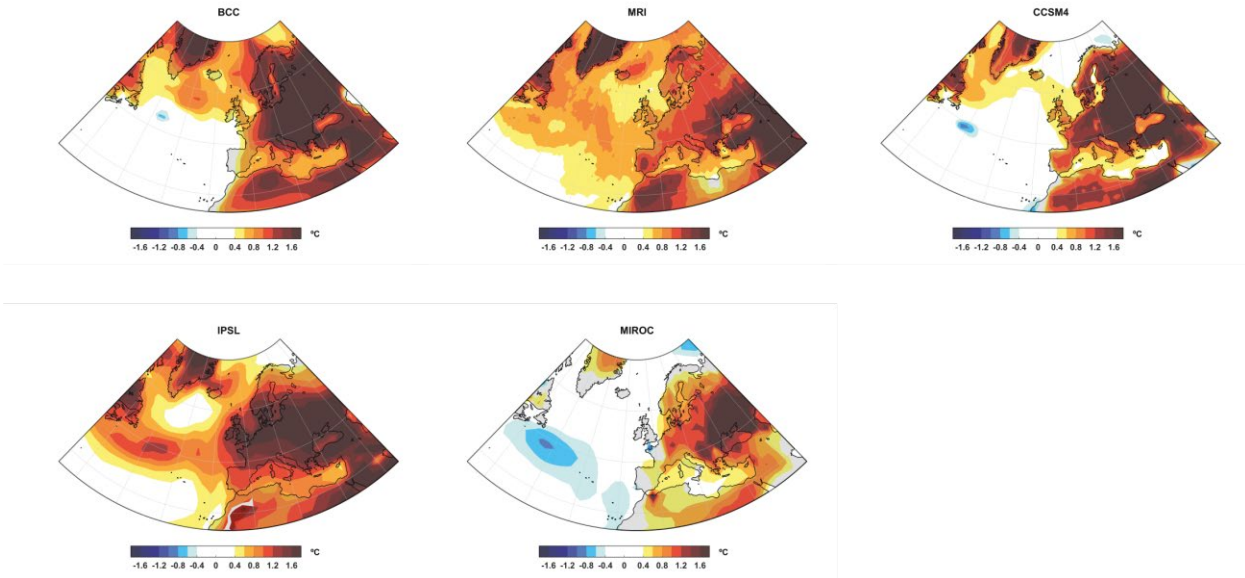

Figure S8: Anomalies in the summer anomalies in the 2 m temperature over the North Atlantic region during the mid-Holocene (when compared to the pre-industrial control period) from five atmosphere-ocean coupled general circulation models (CGCMs) that contributed to the third phase of the Paleoclimate Modelling Intercomparison Project (PMIP3; Braconnot et al. 2012) within the scope of CMIP5. Models are the same than in Figure S7.

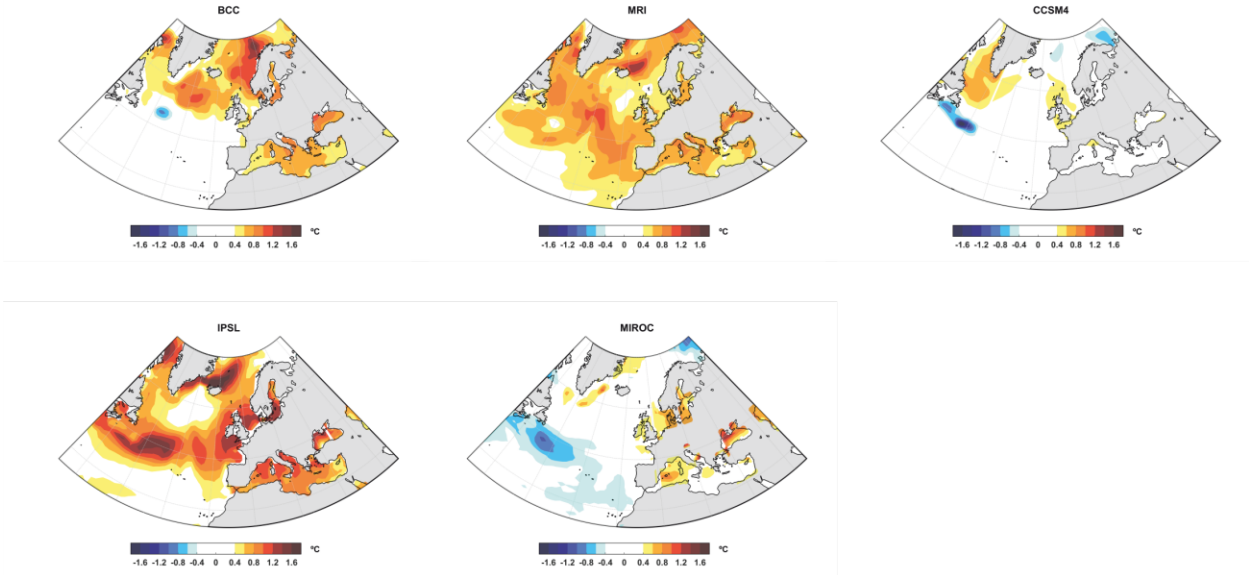

Figure S9: Anomalies in the summer sea surface temperature over the North Atlantic during the mid-Holocene (when compared to the pre-industrial control period) from five atmosphere-ocean coupled general circulation models (CGCMs) that contributed to the third phase of the Paleoclimate Modelling Intercomparison Project (PMIP3; Braconnot et al. 2012) within the scope of CMIP5. Models are the same than in Figure S7.

References Cited

Adão, H., Alves, A., Patricio, J., Neto, J., Costa, M., Marques, J. 2009. Spatial distribution of subtidal Nematoda communities along the salinity gradient in southern European estuaries. Acta Oecol. Int. J. Ecol. 35, 287-300.

Alday, M., Cearreta, A., Cachão, M., Freitas, M.C., Andrade, C., Gama, C., 2006. Micropaleontological record of Holocene estuarine and marine stages in the Corgo do Porto rivulet (Mira River, SW Portugal). Estuarine, Coastal and Shelf Science 66, 532–543.

Amaral, V., Paula, J. 2007. *Carcinus maenas* (Crustacea: Brachyura): influence of artificial substrate type and patchiness on estimation of megalopae settlement. Journal of Experimental Marine Biology and Ecology 346, 21–27.

Berger A., Loutre M.F. 1991. Insolation values for the climate of the last 10 million years. Quaternary Sciences Review, Vol. 10 No. 4, pp. 297-317.

Blaauw, M., Christen, J.A. 2011. Flexible paleoclimate age-depth models using an autoregressive gamma process. Bayesian Anal. 6, no. 3, 457-474.

Bonaventura, D., Cancela da Fonseca, L., Teles-Ferreira, C. 1999. Trophic structure of macrobenthic communities on the Portuguese coast. A review of lagoonal, estuarine and rocky littoral habitats. Acta Oecologica 20, 307-415.

Braconnot, P., Harrison, S. P., Kageyama, M., Bartlein, P. J., Masson-Delmotte, V., Abe-Ouchi, A., Otto-Bliesner, B., Zhao, Y. 2012. Evaluation of climate models using paleoclimate data. Nature Climate Change, 2, 417–424.

Dufresne, J.-L., Foujols, M.-A., Denvil, S., Caubel, A., Marti, O., Aumont, O., Balkanski, Y., Bekki, S., Bellenger, H., Benshila, R., Bony, S., Bopp, L., Braconnot, P., Brockmann, P., Cadule, P., Cheruy, F., Codron, F. F., Cozic, A., Cugnet, D., de Noblet, N., Duvel, J.-P., Ethé, C., Fairhead, L., Fichefet, T., Flavoni, S., Friedlingstein, P., Grandpeix, J.-Y., Guez, L., Guilyardi, E., Hauglustaine, D., Hourdin, F., Idelkadi, A., Ghattas, J., Joussaume, S., Kageyama, M., Krinner, G., Labetoulle, S., Lahellec, A., Lefèbvre, M.-P., Lefèvre, F., Lévy, C., Li, Z. X., Lloyd, J., Lott, F., Madec, G., Mancip, M., Marchand, M., Masson, S., Meurdesoif, Y., Mignot, J., Musat, I., Parouty, S., Polcher, J., Rio, C., Schulz, M., Swingedouw, D., Szopa, S., Talandier, C., Terray, P., Viovy, N. 2013. Climate change projections using the IPSL-CM5 Earth System Model: from CMIP3 to CMIP5, Climate Dynamics, 40, 2123–2165.

França, S., Costa, M.J., Cabral, H.N., 2009. Assessing habitat specific fish assemblages in estuaries along the Portuguese coast. Estuar. Coast. Shelf Sci. 83, 1-12.

Gent PR, Danabasoglu G, Donner LJ, Holland MM, Hunke EC, JayneSR, Lawrence DM, Neale RB, Rasch PJ, Vertenstein M, Worley PH,Yang Z-L, Zhang M. 2011. The community climate system model version 4. Journal of Climate 24, 4973–4991.

Loureiro, I.M., Cabral, M.C., Fatela, F. 2009. Marine influence in ostracod assemblages of the Mira River estuary: Comparison between lower and mid estuary tidal marsh transects. J. Coastal Res., Special issue 56, 1365-1369.

Stuiver, M., Reimer, P.J., Bard, E., Beck, J.W., Burr, G.S., Hughen, K.A., Kromer, B., McCormac, G., van der Plicht, J., Spurk, M., 1998. INTCAL98 radiocarbon age calibration. Radiocarbon 40, 1041-1083.

Sueyoshi, T., Ohgaito, R., Yamamoto, A., Chikamoto, M. O., Hajima, T., Okajima, H., Yoshimori, M., Abe, M., O'ishi, R., Saito, F., Watanabe, S., Kawamiya, M., Abe-Ouchi, A. 2013. Set-up of the PMIP3 paleoclimate experiments conducted using an Earth system model, MIROC-ESM, Geosci. Model Dev., 6, 819–836.

Usoskin IG, Gallet Y, Lopes F, Kovaltsov GA, Hulot G. 2016. Solar activity during the Holocene: the Hallstatt cycle and its consequence for grand minima and maxim. Astron Astrophys, 587, A150.

Xin, X.-G., Wu, T.-W., Zhang, J. 2013. Introduction of CMIP5 experiments carried out with the climate system models of Beijing Climate Center. Adv. Clim. Change Res., 4, 41-49.

Yukimoto, S., Adachi, Y., Hosaka, M., Sakami, T., Yoshimura, H., Hirabara, M., Tanaka, T. Y., Shindo, E., Tsujino, H., Deushi, M. 2012. A new global climate model of the Meteorological Research Institute: MRI-CGCM3 – Model description and basic performance. J. Meteorol. Soc. Jpn., 90A, 23–64.